Journal of Applied Polymer Science

Ion-transport study in nanocomposite solid polymer electrolytes based on chitosan: Electrical and dielectric analysis

Shujahadeen B. Aziz,[1] Zul Hazrin Z. Abidin[2]

[1]Advanced Materials Research Laboratory, Department of Physics, Faculty of Science and Science Education, School of Science, University of Sulaimani, Sulaimani, Kurdistan Regional Government, Iraq

[2]Center for Ionics University of Malaya, Department of Physics, Faculty of Science, University of Malaya, Kuala Lumpur 50603, Malaysia

Correspondence to: S. B. Aziz (E-mail: shujaadeen78@yahoo.com)

ABSTRACT: In this study, $(1.1111-x)(0.9CS–0.1NaTf)—xAl_2O_3(0.02 \leq x \leq 0.1)$ [where CS is chitosan, NaTf is sodium triflate ($NaCF_3SO_3$), and Al_2O_3 is aluminum oxide] nanocomposite solid polymer electrolyte (SPE) films based on CS were prepared by a solution casting technique. X-ray diffraction and scanning electron microscopy analysis revealed that the alumina nanoparticles had a great effect on the structural and morphological behavior of the CS–NaTf (90:10) polymer electrolyte. An investigation of the electrical and dielectric parameters of the nanocomposite SPE films was conducted. Electrical impedance spectroscopy was carried out for this purpose. The relationships between the electrical and dielectric parameters were used to interpret and understand the ion-conduction mechanism. We observed that the direct-current conductivity (σ_{dc}) and dielectric constant followed the same trend with salt concentration. σ_{dc} versus temperature showed the Arrhenius and Vogel-Fulcher-Tammann (VTF) regions. The drops of σ_{dc} at high temperatures were observed for all of the samples. The ion relaxation dynamics were studied from Argand plots. For the first time, we confirmed the existence of a strong experimental relationship between the high-frequency semicircle of the impedance plots and the high-frequency dispersion regions of the alternating-current conductivity (σ_{ac}). The dispersion regions of σ_{ac} were used to study the ion-conduction mechanism. The behavior of the frequency exponent as a function of the temperature was used to interpret σ_{dc} versus the temperature. © 2014 Wiley Periodicals, Inc. J. Appl. Polym. Sci. **2015**, *132*, 41774.

KEYWORDS: biomaterials; biopolymers and renewable polymers; dielectric properties

Received 16 July 2014; accepted 10 November 2014

DOI: 10.1002/app.41774

INTRODUCTION

Dry solid polymer electrolytes (SPEs) have been attracting interest as a safer choice than liquid electrolytes.[1] Pioneering work in the field of SPEs was carried out by Wright *et al.* cited by Singh & Bhat[2] who reported a direct-current conductivity (σ_{dc}) on the order of 10^{-5} S/cm at 330 K in highly crystalline poly ethylene oxide-Sodium thiocyanate (PEO–NaSCN) complexes. SPEs are formed by the dissolution of salts in a polymer matrix. They have received considerable attention as solid electrolyte materials for advanced applications, such as high-energy density batteries, sensors, and fuel cells.[3] The main advantages of SPEs are their good mechanical properties, ease of fabrication into thin films of desirable sizes, and an ability to form good electrode/electrolyte contacts.[4] A recent challenge has been to find a low-cost membrane with a high ionic conductivity (σ) and good dimensional and mechanical stabilities. Although SPEs have many advantages, such as mechanical flexibility and corrosion resistance, they also have some disadvantages, such as a low ionic σ and high crystallinity. Ionic conduction in SPEs is known to take place in the amorphous fraction of the polymer matrix, but the polymers used as hosts in polymer electrolytes are often semicrystalline.[5] Thus, to overcome the disadvantages and improve σ of SPEs, the method that is mostly applied is the addition of plasticizer to improve the ambient ionic σ. Plasticizers can increase the amorphous content of polymer electrolytes and dissociate the ion aggregates present in polymer electrolytes and, thereby, improve the electrical σ of SPE.[6] It is important to note that the σ and mechanical stability of plasticized polymer electrolytes are properties that have a reciprocal effect on each other; that is, the ionic σ in plasticized polymer electrolytes increases at the expense of reduced mechanical strength and vice versa.[7] In addition to a high σ and wide electrochemical stability window, polymer electrolytes must exhibit a high thermal and mechanical performance. These performances can be obtained by the dispersal of nanosize fillers in polymer electrolytes. Since the original work of Weston and

Steele,[8] nanocomposite polymer electrolytes have been studied extensively; that is, nanofiller dispersion is a popular approach for overcoming the shortcomings, such as the mechanical strength. The understanding of the impact of the inorganic filler on the conduction and thermal, mechanical, and electrochemical properties of the polymer electrolytes is still a work in progress.[9] The most used nanoparticles are TiO_2, aluminum oxide (Al_2O_3), SiO_2, MgO, and so forth. The addition of these nanoparticles to SPE has been found to be one of the most effective routes for achieving balanced characteristics of ionic σ and mechanical stability.[5] Recently, Malathi *et al.*[10] and Prajapati *et al.*[11] considered complex permittivity parameters in explaining the ionic σ of polyvinyl alcohol-based SPEs. Pradhan *et al.*[12] and Sengwa *et al.*[13] also used dielectric analysis to understand the σ behavior in nanocomposite SPEs. An extensive and intensive survey of literature indicated that very little work has been done on the dielectric properties of ion-conducting SPEs and nanocomposite electrolytes. Even the mechanism of ion conduction in SPEs is still not well understood. Hence, it is important to understand the ion-transport behavior in solid and nanocomposite polymer electrolytes. The dielectric parameters associated with relaxation processes are of particular significance in ion-conducting polymers, where the dielectric constant (ε') plays a fundamental role that shows the ability of a polymer material to dissolve salts.[14] Thus, the main objective of this study was to demonstrate the role of ε' on σ_{dc} and the effect of electrode polarization (EP) on the alternating-current conductivity (σ_{ac}) dispersion in nanocomposite polymer electrolytes based on chitosan (CS). In this study, for the first time, we showed some important relationship between the electrical and dielectric parameters; this is very useful for understanding the ion-conduction mechanism in nanocomposite SPEs.

EXPERIMENTAL

Raw Materials

CS from crab shells (≥75% deacetylated, average molecular weight = 1.1×10^5) was procured from Sigma and sodium triflate (NaTf or $NaCF_3SO_3$) and Al_2O_3 (size < 50 nm) were supplied by Sigma Aldrich. Acetic acid (1%) was prepared with glacial acetic acid solution and used as the solvent to prepare nanocomposite SPEs.

Preparation of the Solid and Nanocomposite Polymer Electrolytes

The SPE films were prepared by the solution casting technique. For this purpose, 1 g of CS was dissolved in 100 mL of 1% acetic acid solution. The mixture was stirred continuously with a magnetic stirrer for several hours at room temperature until the CS powder completely dissolved in the acetic acid solution. To this solution, 10 wt % NaTf was added, and the mixture was stirred continuously until a homogeneous solution was obtained. The solution of CS–NaTf (90:10) was then cast into a clean and dry Petri dish and allowed to evaporate at room temperature to obtain a solvent-free film. To prepare the nanocomposite solid polymer electrolytes (NCSPEs), initially the CS and NaTf (90:10) were dissolved in acetic acid to obtain homogeneous solutions, as mentioned previously. The Al_2O_3 was first dispersed in 20 mL of acetic acid solution and stirred. The Al_2O_3 concentrations were varied from 2 to 10 wt %. The Al_2O_3 dispersoids were mixed with CS–NaTf (90:10) solutions and then continuously stirred. The solutions were then cast into different clean and dry Petri dishes and allowed to evaporate at room temperature until solvent-free NCSPE films were obtained. The films were kept in desiccators with a blue silica gel desiccant for further drying. Table I shows the concentration of the prepared $(1.1111-x)$(0.9CS–0.1NaTf)—x Al_2O_3 $(0.02\le x\le 0.1)$ NCSPEs.

Table I. Composition of the $(1.1111-x)$(0.9CS–0.1NaTf)—$x$$Al_2O_3$ $(0.02\le x\le 0.1)$ NCSPEs

Designation	CS–NaTf (90:10) (g)	Al_2O_3 (wt %)	Al_2O_3 (g)
CSNB1	1.1111	2.0	0.0227
CSNB2	1.1111	4.0	0.0463
CSNB3	1.1111	6.0	0.0709
CSNB4	1.1111	8.0	0.0966
CSNB5	1.1111	10	0.1235

CSNB1 to CSNB6 represent the sample codes of the NCSPE compositions of $(1.1111-x)$(0.9CS–0.1NaTf)—$x$$Al_2O_3$ $(0.02\le x\le 0.1)$.

X-ray Diffraction (XRD) and Morphology Characterization

In this study, XRD was used to reveal the nature of the complexed film, whether amorphous or crystalline. XRD was carried out with a Siemens D5000 X-ray diffractometer with an operating voltage and current of 40 kV and 40 mA, respectively. The wavelength of the monochromatic X-ray beam was 1.5406 Å, and the glancing angles were in the range $5^\circ\le 2\theta\le 80^\circ$ with a step size of 0.1°. The combined usage of scanning electron microscopy (SEM)–energy-dispersive analysis of X-rays (EDX) was an attempt to understand the structural and compositional complexity of the samples. A scanning electron micrograph was taken with a Leica 440 scanning electron microscope to study the morphological appearance. The microscope was fitted with EDX [Oxford Instrument (LINK ISIS)] to detect the overall chemical compositions of the NCSPEs. Before observation, the NCSPE films were attached to an aluminum holder with a conductive tape and then coated with a thin layer of gold.

Electrical Impedance Spectroscopy (EIS)

Complex impedance (Z^*) spectroscopy gives information on the electrical properties of materials and their interface with electronically conducting electrodes. The NCSPE films were cut into small discs (2 cm in diameter) and sandwiched between two stainless steel electrodes under spring pressure. The average thicknesses of the NCSPE films were between 125 and 127 μm. The impedance of the films was measured in the frequency range from 50 Hz to 1000 kHz with a HIOKI 3531 Z Hi-Tester. which was interfaced with a computer. Measurements were also made at temperatures ranging between 303 and 363 K. The software controlled the measurements and calculated the real (Z') and imaginary (Z'') parts of the impedance. The Z' and Z'' data are presented as a Nyquist plot, and the bulk resistance was obtained from the intercept of the plot with the real impedance axis. σ_{dc} was calculated from the following equation:[15]

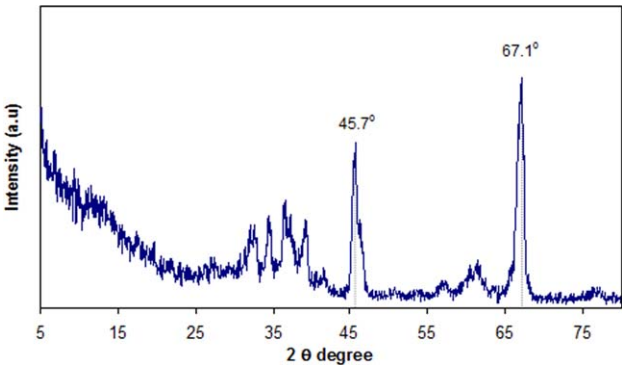

Figure 1. XRD patterns of the pure Al_2O_3 nanoparticles. [Color figure can be viewed in the online issue, which is available at wileyonlinelibrary.com.]

$$\sigma_{dc} = \left(\frac{1}{R_b}\right) \times \left(\frac{t}{A}\right) \quad (1)$$

where t is the film's thickness, R_b is bulk resistance and A is its area.

Z' and Z'' of Z^* were also used for the evaluation of ε', σ_{dc}, and the real (M') and imaginary (M'') parts of the complex electric modulus (M^*) with the following equations:[16,17]

$$\varepsilon' = \frac{Z_i}{\omega C_o (Z_r^2 + Z_i^2)} \quad (2)$$

$$\sigma_{ac} = \left[\frac{Z'}{Z'^2 + Z''^2}\right] \times \left(\frac{t}{A}\right) \quad (3)$$

$$M' = \omega C_o Z_i \quad (4)$$

$$M'' = \omega C_o Z_r \quad (5)$$

where C_o is the vacuum capacitance and is given by $\varepsilon_o A/t$, where ε_o is the permittivity of free space and is equal to 8.85×10^{-12} F/m. The angular frequency (ω) is equal to $\omega = 2\pi f$, where f is the frequency of the applied field.

RESULTS AND DISCUSSION

Structural and Morphological Analysis

XRD is a powerful tool for investigating the crystallinity and structural changes in membranes of solid and nanocomposite polymer electrolytes. Figure 1 shows several crystalline peaks around 32, 34.4, 36, 39, 41, 45.7, 61, and 67.1° for pure Al_2O_3. The XRD pattern of the Al_2O_3 nanoparticles depicted in Figure 1 was very similar to the Al_2O_3 pattern reported in the literature.[18] The sharp crystalline peaks at 45.7 and 67.1° revealed that the Al_2O_3 nanoparticles were almost crystalline materials.

To observe the effect of the Al_2O_3 nanoparticles on the crystalline structure of the SPEs based on CS–NaTf (CSB6), XRD was carried out. Details of the XRD study of CS–NaTf (90:10) were given in our previous work.[19] Figure 2 displays the XRD pattern of CS–NaTf (90:10) with various concentrations of Al_2O_3 (2–10 wt %). With the addition of Al_2O_3 nanoparticles to CS–NaTf (90:10), the crystalline peaks of CS–NaTf SPE became broader and less sharp, especially at 4 wt %. From the XRD results of these nanocomposites, it was clear that at low filler concentrations (2–4 wt %), the amorphous region was dominant. However, at high filler concentrations (6–10 wt %), the crystalline peaks of the CS polymer became sharp, and the Al_2O_3 crystalline peaks at 45.7 and 67.1° were appeared. According to Raghavan *et al.*,[20] the broadening and lowering of the intensity of the diffraction peaks on the incorporation of the nanosized ceramic fillers indicated an amorphous enhancement. The reduction in the crystallinity resulted from the complex formation between the polar groups of the polymer and the surface groups of the nanosized ceramic fillers (OH); this retarded the ordering of the crystalline regions in the polymer electrolyte. The higher amorphous nature of the electrolyte resulted in a higher σ of the sample. On the addition of more than 4 wt % Al_2O_3, the overall crystalline structure of the NCSPEs increased.

To support the XRD results, SEM and EDX were carried out on the NCSPEs. From Figure 3, it was obvious that the NCSPEs containing 2 and 4 wt % were almost smooth, and the Al_2O_3 nanoparticles were well distributed without the appearance of any aggregated spots of Al_2O_3 nanoparticles. However, from 6 to 10 wt % Al_2O_3, the surface morphology showed Al_2O_3 aggregates on the top surface. As a whole, the distribution of Al_2O_3 nanoparticles were homogeneous and uniform when the amount of filler was less than 6 wt %. We observed from the EDX result that the main peak was attributable to Al_2O_3. The results of SEM and EDX analysis of these nanocomposites revealed that the Al_2O_3 nanoparticles were finely dispersed at low concentrations (2–4 wt %), whereas a lot of white aggregated clusters were formed and appeared on the surface of the samples at high alumina concentrations (6–10 wt %). These white aggregates were ascribed to the phase separation of alumina from the polymer matrix because the aggregated nanoparticles were not compatible with the polymer matrix at higher filler concentrations.[21] Thus, the SEM and EDX analyses of these nanocomposites greatly supported the XRD results.

Composition Dependence of ε' and σ_{dc}

Figure 4 shows the frequency dependence of ε' for different alumina concentrations. ε' increased with decreasing frequency. This was because at low frequency, the dipoles and charge carriers had sufficient time to orient in the direction of the applied electric field. Consequently, large amounts of charge carriers built up at the electrode/electrolyte interface and produced EP;

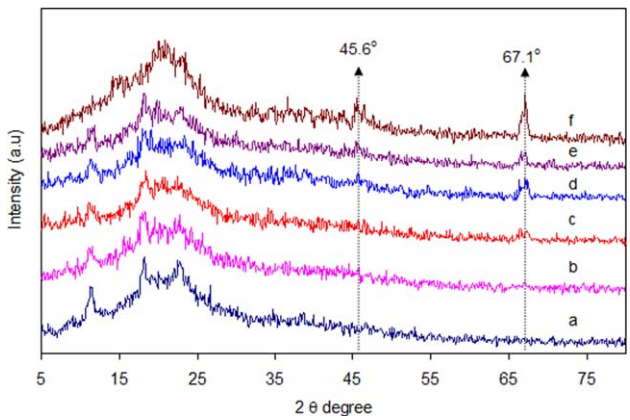

Figure 2. X-ray diffractograms of (a) CS–NaTf (90:10), (b) CSNB1, (c) CSNB2, (d) CSNB3, (e) CSNB4, and (f) CSNB5. [Color figure can be viewed in the online issue, which is available at wileyonlinelibrary.com.]

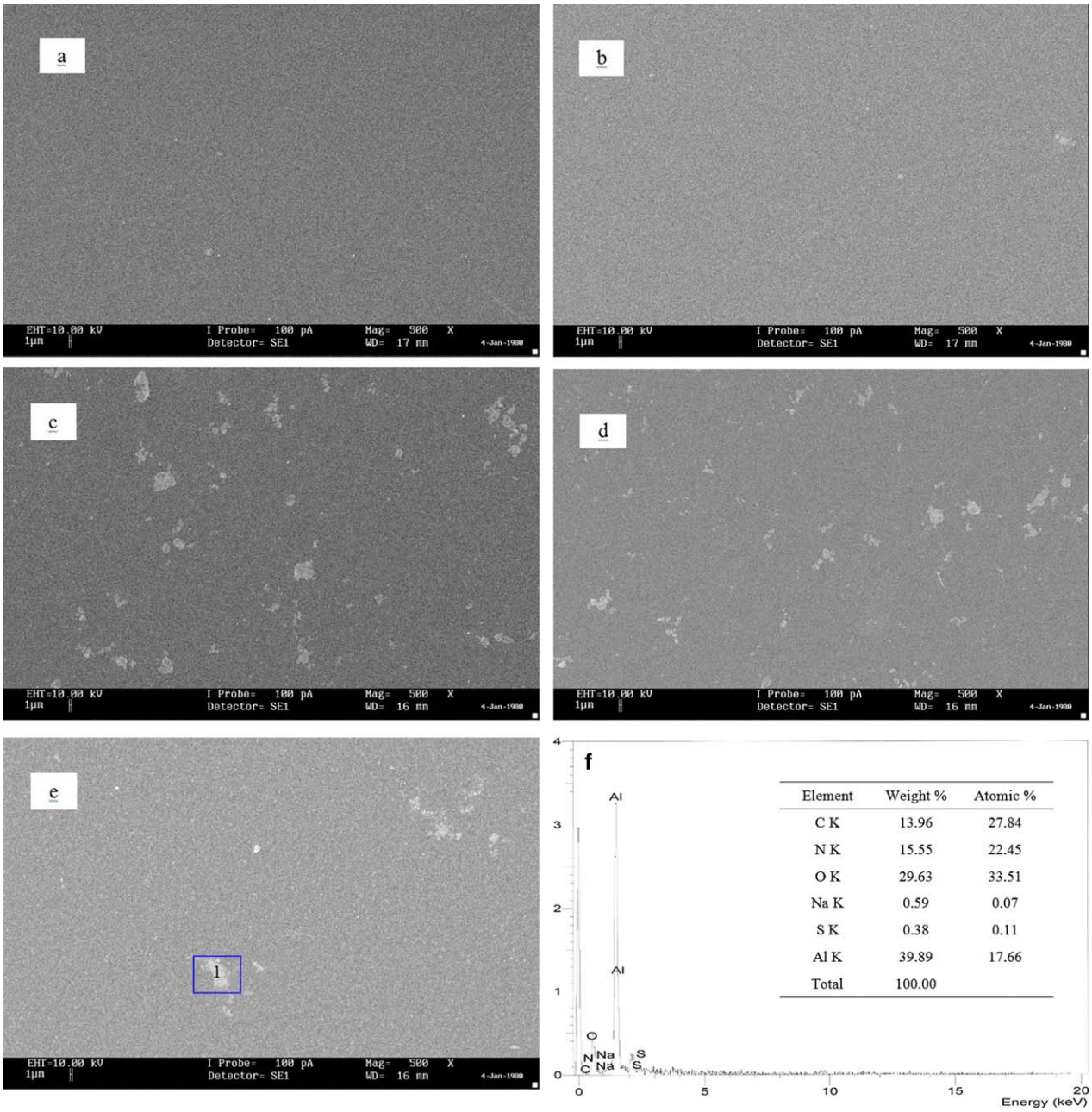

Element	Weight %	Atomic %
C K	13.96	27.84
N K	15.55	22.45
O K	29.63	33.51
Na K	0.59	0.07
S K	0.38	0.11
Al K	39.89	17.66
Total	100.00	

Figure 3. SEM images of (a) CSNB1, (b) CSNB2, (c) CSNB3, (d) CSNB4, and (e) CSNB5 and (f) EDX for the spot in box 1. [Color figure can be viewed in the online issue, which is available at www.interscience.wiley.com.]

this suppressed the high-frequency dielectric properties (bulk properties). It was obvious that ε' increased from 2 to 4 wt % and then decreased at 6 wt %. After that, ε' exhibited a second increase from 8 to 10 wt %. The high-frequency part of ε', which appeared as a single bundle, show similar behavior as the low part of ε' with the alumina concentration.

Figure 5 represents the separated bulk ε' (high-frequency region) for various concentrations of alumina nanoparticles. It was obvious that the bulk ε', like the low-frequency region, was strongly affected by the alumina concentration. The high-frequency region of ε' was important for understanding the ion-conduction mechanism because the bulk σ_{dc} also was related to the high-frequency semicircle of the impedance plots. The extrapolation of the high-frequency ε' regions to the y axis was used to obtain the ε' values of the samples. We achieved the complete relationship between the bulk σ_{dc} and bulk ε' by plotting both of them on the same figure, as shown later.

The variation of σ_{dc} and ε' of CS–NaTf (90:10) with various concentrations of Al_2O_3 nanoparticles is depicted in Figure 6. σ_{dc} and ε' increased with the addition of 2–4 wt % Al_2O_3 nanoparticles, and thereafter, they decreased at 6 wt %. Then, they increased again at high filler concentrations (8–10 wt %). It was obvious that the behavior of bulk ε' and bulk σ_{dc} was almost the same with Al_2O_3 concentration. These results reveal the role

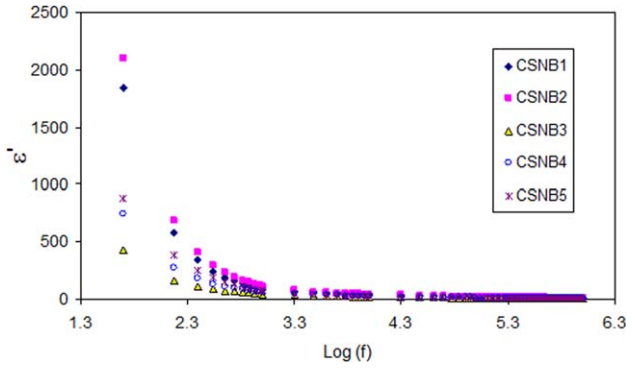

Figure 4. Frequency dependence of ε' for $(1.1111-x)$(0.9CS–0.1NaTf)—$x$$Al_2O_3$ $(0.02 \le x \le 0.1)$ NCSPEs. [Color figure can be viewed in the online issue, which is available at wileyonlinelibrary.com.]

of ε' enhancement on σ_{dc} in the nanocomposite polymer electrolytes; this was interpreted as follows. The ionic σ of NCSPEs could be described by the following relation:

$$\sigma = \sum_i n_i q_i \mu_i \tag{6}$$

where n_i is the concentration of the charge carriers, q is the electron charge, μ_i is the mobility of ions, and i is the type of ion. It was clear from the previous relation that σ depended on the charge carrier concentration (n), and the mobility of the ionic species in the system. n depends on both the dissociation energy (U) involved and ε' as[22,23]

$$n = n_o \exp(-U/\varepsilon' K_B T) \tag{7}$$

where K_B is Boltzmann's constant and T is the absolute temperature and no is a pre-exponential constant. Because of the direct relationship between ε' and the charge, an increase in ε' is ascribed to the increase in the amount of charge in the sample; that is, an increase in ε' represents a fractional increase in the charges within the electrolyte. Now, it is clear from eq. (6) that σ depends on n, and the mobility of the ionic species in the system. As shown by eq. (7), n increases with increasing ε'. Consequently, σ increases according to eq. (6). The previous equations indicate the fact that dielectric analysis is an informative technique for studying the σ behavior of polymer electrolytes. The nonmonotonic behavior of σ_{dc} and ε' upon the increment of the alumina contents can be explained by two physical situations, namely, the space-charge-induced enhancement effect and the blocking effect. The space-charge-induced enhancement effect provides local electric fields, which accelerate the transport of conduction ions and thereby increase σ. This effect has been observed and reported in numerous composite systems.[24] The blocking effect, on the other hand, impedes the flow of conduction ions and, thereby, reduced σ, as depicted in Figure 6. Tan *et al.*,[25] reported that at higher filler concentrations, more abundant alumina nanoparticles could make long polymer chains more immobilized; that is, they reduced the segmental mobility and thus led to a decreasing σ. The second increase in σ_{dc} and ε' (from 8 to 10 wt %) was explained on the fact that at higher filler contents, the filler grains got close enough to each other at higher concentrations so that the high conducting regions in the vicinity of the grain surfaces started to get interconnected. The migrating ionic species could then travel along and between these interconnected high-conducting pathways and give rise to the second increase in σ_{dc} and ε'.[26] Compared to the CS–NaTf (90:10) system, σ_{dc} of the $(1-x)$(0.9CS–0.1NaTf)—$x$$Al_2O_3$ $(0.02 \le x \le 0.1)$ compositions was increased by two orders. The increase in σ_{dc} was ascribed to the ε' enhancement, as depicted in Figure 6. ε' was directly related to the capacitance (C) of the sample ($\varepsilon' = C/C_o$). The high ε' of the sample indicated a high charge carrier density.

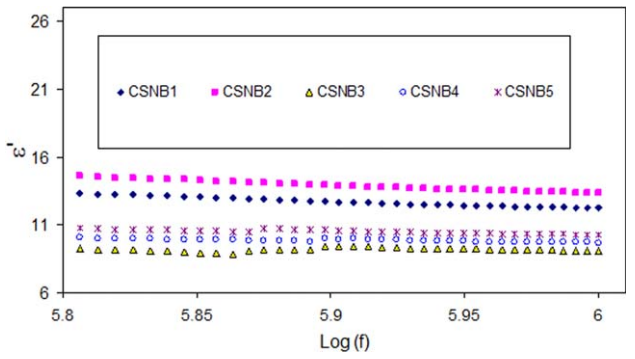

Figure 5. Frequency dependence of the bulk ε' for $(1.1111-x)$(0.9CS–0.1NaTf)—$x$$Al_2O_3$ $(0.02 \le x \le 0.1)$ NCSPEs. [Color figure can be viewed in the online issue, which is available at wileyonlinelibrary.com.]

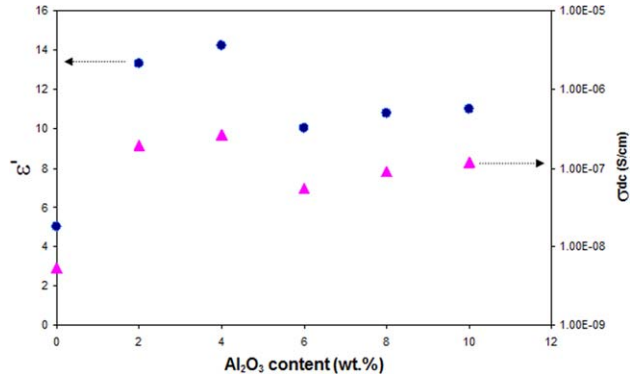

Figure 6. Dependence of the bulk ε' (ε' at 1 MHz) and σ_{dc} of CS–NaTf (90:10) on the Al_2O_3 concentration. [Color figure can be viewed in the online issue, which is available at wileyonlinelibrary.com.]

Temperature Dependence of ε' and σ_{dc}

Figure 7 shows the temperature-dependent σ of different nanocomposite solid electrolyte samples. It was clear from the plots that the temperature dependence of σ followed the Arrhenius behavior for the compositions from 2 to 10 wt % at low temperatures (303–333 K). However, they did not follow the Arrhenius behavior for all of the compositions at higher temperatures. Similar behaviors were reported for PEO–LiTf–Al_2O_3 composite polymer electrolytes.[26] The bend in the curve has been observed in ionically conducting polymers and has been explained as invoking the concept of free volume.[27] It is interesting to note that the curve obtained for the highest filler concentration (10 wt %) seemed to maintain linearity quite well up to the highest temperatures. According to Osińska *et al.*,[28] the high filler load helps to prevent ionic transport deterioration at higher temperatures. They explained this phenomenon by assuming that an additional ion-transport mechanism occurred

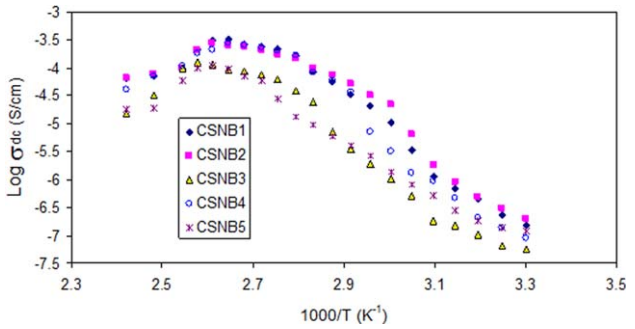

Figure 7. Temperature dependence of σ_{dc} of $(1.1111 - x)(0.9CS–0.1NaTf)–xAl_2O_3$ $(0.02 \leq x \leq 0.1)$ NCSPEs. [Color figure can be viewed in the online issue, which is available at wileyonlinelibrary.com.]

when the filler particles became more and more packed in the composite membrane. The decrease of σ_{dc} at a particular temperature for all of the compositions again was ascribed to the phase transition of the alumina nanoparticles. It is well known that ceramic fillers exhibiting a ferroelectric-to-paraelectric phase transition at the characteristic temperature, which is known as the Curie temperature (T_c). Below T_c, the ferroelectric materials showed spontaneous polarization. Under the influence of the electric field, the dipole moments were able to follow the applied field and contributed to the overall polarization of the system. However, as the temperature approached T_c, a transition took place from order to disorder in the crystal structure of the ceramic filler and made no more contribution to σ enhancement.[29] Jiansirisomboon and Watcharapasorn[30] reported the T_c of the nanocomposite $BaTiO_3–Al_2O_3$ in the temperature range from 118 to 125°C using dielectric spectroscopy; this was very close to the temperature at which the σ values of the samples dropped in this study.

An ε' study at different temperatures gave further information on the relationship between the bulk σ_{dc} and ε'. Figure 8 shows ε' as a function of the frequency at different temperatures. As shown, with increasing temperature, ε' also increased. The large value of ε' at low frequency was attributable to the EP effect, which suppressed the high-frequency ε' to a single curve.

Figure 9 shows the frequency dependence of the bulk ε' at selected temperatures. It was interesting that the bulk ε' was

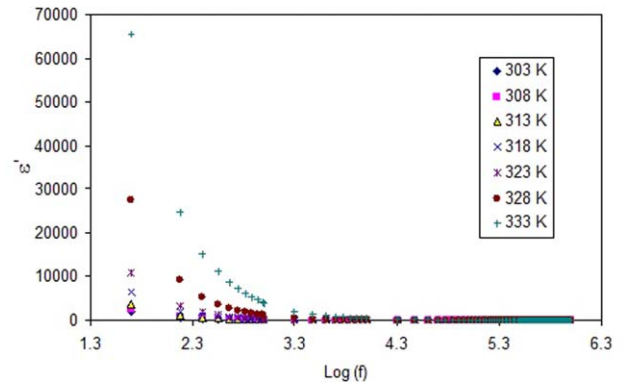

Figure 8. Frequency dependence of ε' at different temperatures for the CSNB2 system. [Color figure can be viewed in the online issue, which is available at wileyonlinelibrary.com.]

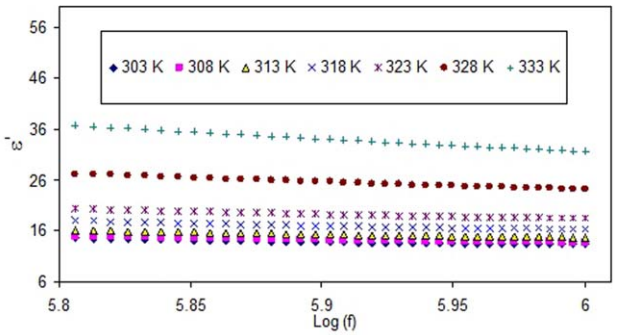

Figure 9. Frequency dependence of the bulk ε' at different temperatures for the CSNB2 system. [Color figure can be viewed in the online issue, which is available at wileyonlinelibrary.com.]

also temperature-dependent like the low-frequency ε'. We know that the bulk σ_{dc} and bulk ε' were extracted from the high-frequency semicircle. Thus, σ_{dc} must also have been strongly ε' dependent at these different temperatures. The slight inclination of the bulk ε' was ascribed to the EP dominance at high temperatures; this could be seen in the Cole–Cole ($Z''–Z'$) study discussed in later sections. Z_i refers to the imaginary part of complex impedance, while Z_r refers to its real part.

Figure 10 shows σ_{dc} as a function of the bulk ε' at different temperatures. It was obvious from the plot that the bulk σ_{dc} smoothly increased with increasing bulk ε', and the increase in ε' indicated an increase in n at different temperatures. From the fundamental point of view, the dielectric relaxation and ion-conduction mechanism in solids are the most intensively researched topics in condensed matter physics and especially ionic transport in polymer electrolytes. Ion transport is complex and depends on factors such as the salt concentration and ε' of the host polymer.[31] ε' analysis provides valuable information about the understanding of ion transport in SPEs. An increase in ε' at higher temperatures can be ascribed to the fact that the movement of polymer chain segments and side groups become easier at elevated temperatures, and thus, the dissociation of ion pairs increases. This results in the increase in σ_{dc}.[19] Thus, the dependence of the bulk σ_{dc} and ε' (Figure 6) on the Al_2O_3 concentration, together with the smooth curve between σ_{dc} and ε' (Figure 10), confirmed that σ_{dc} was strongly ε' dependent in the NCSPEs. Recently, Petrowsky and Frech[32,33] hypothesized that σ_{dc} is not only a function of temperature but is also dependent on ε' in organic liquid electrolytes. The results of this study revealed the applicability of the Petrowsky and Frech hypothesis for nanocomposite solid electrolytes based on CS. Extra research work is required to show the validity of the relationship between σ_{dc} and ε' in solid and nanocomposite polymer electrolytes, and the reformulation of the Arrhenius equation in another form, which must contain both the temperature and ε', is required. From the results of this study, we understood that ion transport is a complicated subject in NCSPEs as a branch of condensed matter physics.

Electric Modulus Analysis of the CSNB2 System: Relaxation Processes

The usefulness of an electric modulus representation is to suppress the signal intensity associated with the EP effect). Thus,

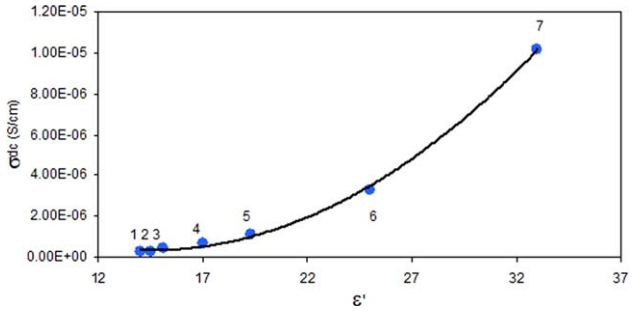

Figure 10. σ_{dc} dependence on ε' at (1) 303, (2) 308, (3) 313, (4) 318, (5) 323, (6) 328, and (7) 333 K for the CSNB2 system. [Color figure can be viewed in the online issue, which is available at wileyonlinelibrary.com.]

the electric modulus spectra provide an opportunity to investigate σ and its associated relaxation in ionic conductors and polymers. The variation of M' as a function of the frequency at selected temperatures is presented in Figure 11. Because of the EP effect, the value of M' was very small at low frequencies. It was clear that the value of M' increased with increasing frequency. The observed dispersion was mainly due to σ relaxation spread over a range of frequencies and indicated the presence of the relaxation time; this should have been accompanied by a loss peak in the diagram of M'' versus frequency.[17]

The variation of M'' is shown in Figure 12. It is obvious from the figure that the maximum peak shifted to the higher frequency side with increasing temperature. The broad and asymmetric of peaks on both sides of the maxima predicted the non-Debye behavior. The region on the left of the peak determined the range in which charge carriers were mobile over long distances, accumulated at electrode/electrolyte interface, and thus contributed to the EP effect, whereas the region to the right was where carriers were confined to potential wells being mobile over short distance and resulting the dispersion in σ_{ac}.[17,34] That is, the appearance of clear relaxation peaks in the M'' spectra resulted in a distinguishable alternating-current (ac) dispersion, as discussed later. The asymmetric nature of the peaks indicated non-Debye relaxation.

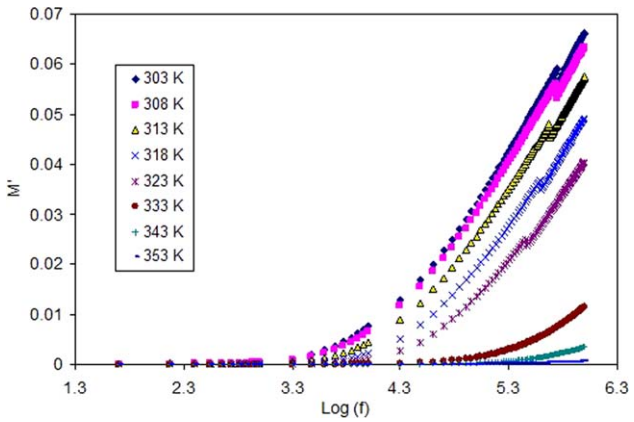

Figure 11. Frequency dependence of M' at different temperatures for a CSNB2 sample. [Color figure can be viewed in the online issue, which is available at wileyonlinelibrary.com.]

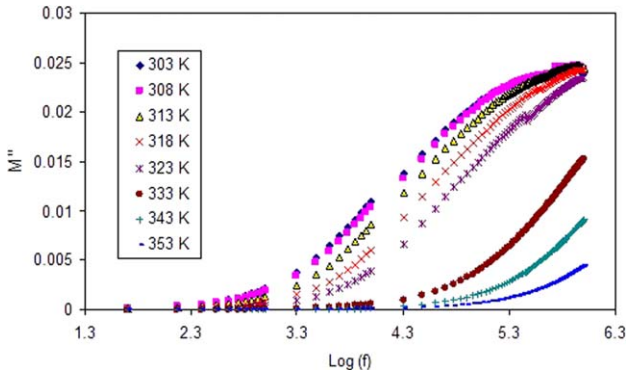

Figure 12. Frequency dependence of M'' at different temperatures for a CSNB2 sample. [Color figure can be viewed in the online issue, which is available at wileyonlinelibrary.com.]

Figure 13 shows the Argand plots at different temperatures. It was obvious that the Argand plots exhibited incomplete semicircular arcs. This confirmed the fact that the relaxation processes were non-Debye type (single relaxation time) in the studied system (CSNB2). Debye relaxation denotes a system with a single relaxation time. In the Debye model, all dipoles must be identical. Thus, Debye relaxation is the dielectric relaxation response of an ideal, noninteracting population of dipoles to an alternating external electric field.[35] In polymer electrolytes under an alternating external electric field, a different polarization mechanism, such as electronic, dipolar, and ionic polarization, occurs. Thus, a distribution of relaxation times will occur in polymer electrolytes. With increasing temperature, the Argand curves shifted toward the origin. The deviation of the Argand plots from the semicircular shape were ascribed to increasing ion conduction and the distribution of relaxation times. Moreover, with increasing temperature, the M''–M' plot deviated more from the semicircular arc. This was ascribed to the increase in σ and the disappearance of the high-frequency semicircle. This was also deduced from the M' and M'' equations:

$$M' = \omega C_o Z_i$$

$$M'' = \omega C_o Z_r$$

Correlation Between the Impedance Plots and the σ_{ac} Dispersion

The correlation of the dielectric properties with the electrical σ is important for understanding the ion-conduction mechanism in solid and nanocomposite-based polymer electrolytes. The EP in a polymer electrolyte is one of the most undesired effects in low-frequency dielectric spectroscopy; it occurs because of the blocking of charges at the sample/electrode interface.[36] In polymer electrolytes containing a low salt concentration, a high-frequency semicircle and a spike region can be observed. The electrical properties associated with the high-frequency semicircle are important because they represent the bulk and intrinsic properties of the material. One of the main advantages of frequency-dependent measurements are that the contributions of the bulk materials (high-frequency region) and the EP (low-frequency spike region) effects can easily be represented.[37] Thus, the EIS technique becomes very efficient and easy because, in frequency-dependent measurements, the bulk and interface have

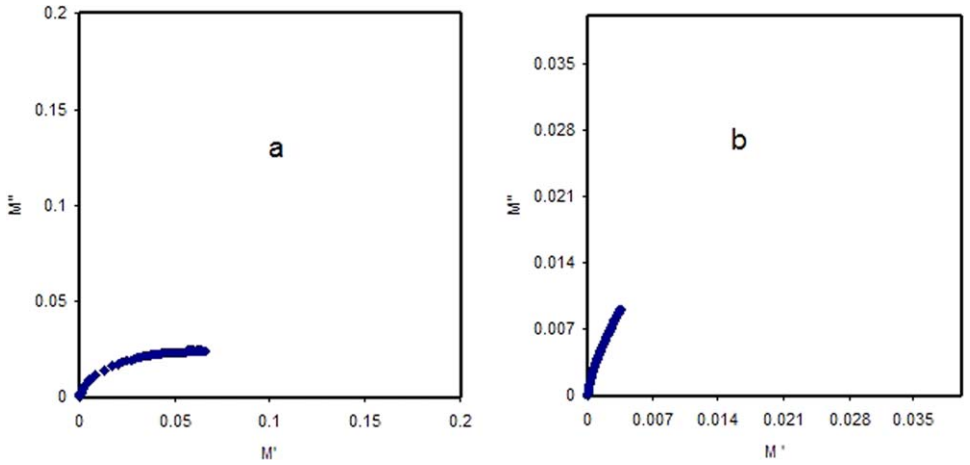

Figure 13. Argand plots for NCSPE (CSNB2) at (a) 303 and (b) 343 K. [Color figure can be viewed in the online issue, which is available at wileyonlinelibrary.com.]

different polarization properties and, therefore, can be separated.

Figure 14 shows the Nyquist plot for NCSPE based on CSNB2. At low temperature (303 K), two regions were observed. The low-frequency region was due to the charge diffusion and accumulation at the electrode/electrolyte interface (EP effect); this produced an electrical double-layer *C*. However, the high-frequency region (high-frequency semicircle); that is, the bulk properties of the material represented the charge-transfer process in the bulk of the material.[38] It was found that with an increase in the temperature to 343 K, the semicircle disappeared. This suggested that only the resistive component of the polymer prevailed.

Figure 15(a–c) shows the σ_{ac} spectra for the CSNB2 sample at selected temperatures. The σ_{ac} plot consisted of three regions at low temperatures in the measured frequency range. The low-frequency region due to the EP effect was followed by a plateau due to σ_{dc} and the high-frequency region, which was an important part of our study, was due to bulk σ_{ac}. We observed that the low-frequency region (EP) became prominent and shifted to the high-frequency part as the temperature increased. The direct correlation between the impedance plots and σ_{ac} spectra revealed that when the high-frequency semicircle (bulk) of the impedance plots disappeared, the high-frequency σ_{ac} dispersion also diminished. These results specifies that the σ_{ac} dispersion was a bulk property of the material and was important for characterizing the type of ion conduction in the bulk of the material via the calculation of the σ_{ac} frequency exponent (*s*). At low temperatures, a clear and distinguishable σ_{ac} dispersion was observed for these solid electrolyte systems. The strong dependence of σ_{ac} on the frequency in the high-frequency region was typical of highly correlated ionic motion in disordered solid electrolytes. It has been reported that the dispersion in σ is direct evidence for the hopping of charge carriers. The dispersion in σ will occur when the carriers are not free to move throughout the sample.[39] Thus, the existence of these ac dispersion region in the σ_{ac} spectra in this study revealed the fact that

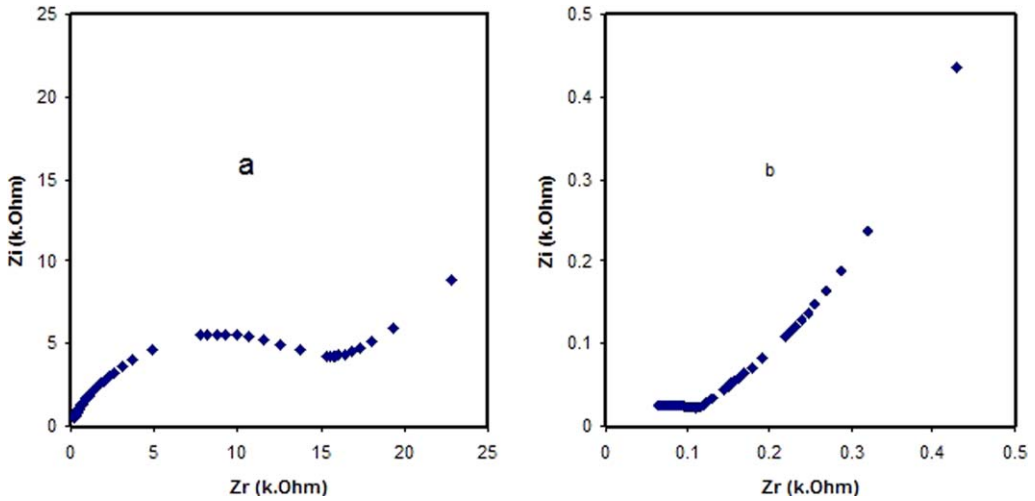

Figure 14. Impedance plots for the NCSPE (CSNB2) system at (a) 303 and (b) 343 K. [Color figure can be viewed in the online issue, which is available at wileyonlinelibrary.com.]

the Jonschers power law could be applicable and the *s* could be used to characterize the model of ion conduction in these NCSPEs. At higher temperatures, only a spike region (EP) was observed. These results indicate the fact that the ac dispersion was a bulk property of the material. It is interesting to note that at high temperatures, the EP effect reduced the ac dispersion. At these temperatures, the ionic σ was high enough to produce a significant build up of charges at the electrodes (EP effect); this reduced the effective applied field across the sample and, hence, the apparent σ.[40] Thus, the EP region could affect the ion distribution. From the experimental results of this study, we concluded that the σ_{ac} dispersion, which is the subject of research by a lot of scientists and explained by many models, was directly related to the existence of the high-frequency semicircle in impedance plots. The calculated *s* from the dispersion regions was used to characterize the type of ion-conduction model in the CSNB2 system.

Figure 16 shows the temperature dependence of *s* for the CSNB2 system. It was obvious that the s value decreased to a minimum value with increasing temperature. The behavior of *s* with temperature could be explained by the correlated barrier hopping (CBH) model.[41,42] The CBH model describes the ion transport between localized states due to hopping over the potential barriers and predicts a decrease in the value of s with increasing temperature,[42] as depicted in Figure 16. Thus, the CBH model is the best model for this NCSPE (CSNB2) system.

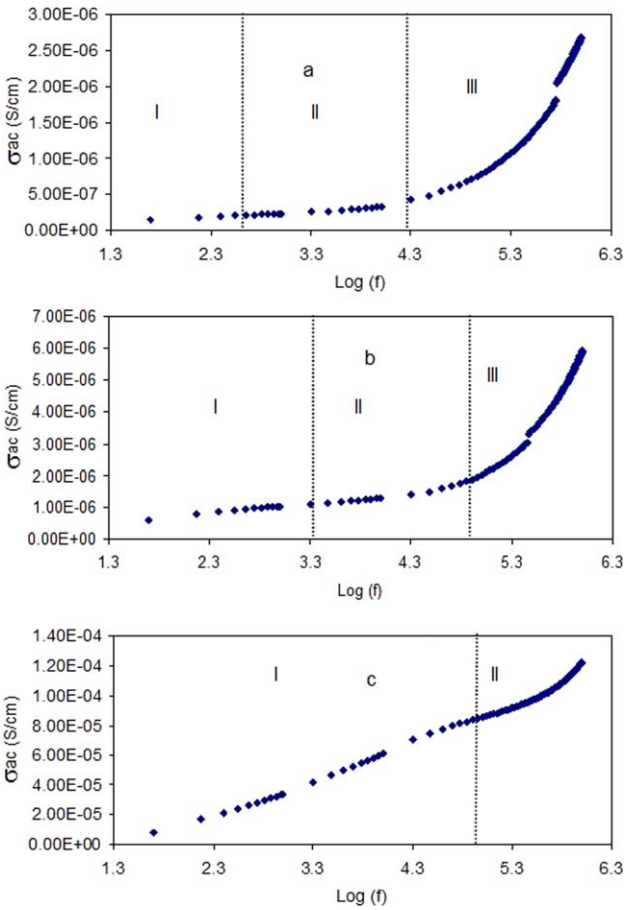

Figure 15. σ_{ac} spectra for the NCSPE (CSNB2) system at (a) 303, (b) 323, and (c) 353 K. [Color figure can be viewed in the online issue, which is available at wileyonlinelibrary.com.]

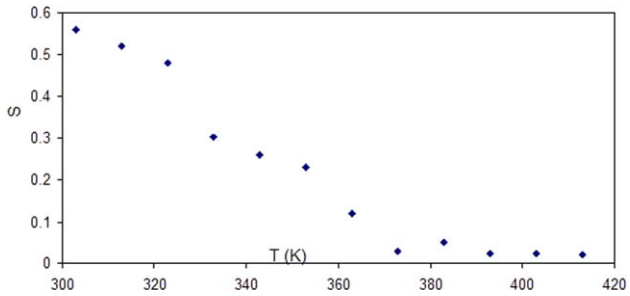

Figure 16. Temperature dependence of *s* for the CSNB2 system. [Color figure can be viewed in the online issue, which is available at wileyonlinelibrary.com.]

CONCLUSIONS

In this study, some noticeable and interesting conclusions about the structural and electrical behavior of the NCSPE films based on CS was obtained. The XRD results revealed that the amorphous region increased upon the addition of Al_2O_3 to 4 wt % and, thereafter, decreased. The SEM analysis strongly supported the XRD results. On the basis of the electrical results, it appeared that the ion-conduction mechanism was not only temperature-dependent but was more complex and was a function of both ε' and temperature. We was observed that σ_{dc} and ε' followed the same trend with the salt concentration and temperature. σ_{dc} versus temperature showed the Arrhenius and VTF regions. The drops in σ_{dc} at high temperatures for all of the samples were ascribed to T_c of the Al_2O_3 nanoparticles. The incomplete semicircle of the Argand plots revealed the non-Debye type relaxation in NCSPEs. From the impedance plots and σ_{ac} study, we concluded that the high-frequency ac dispersion was strongly related to the existence of the high-frequency semicircle of the impedance plots. The dispersion regions of σ_{ac} were used to study the direct-current ion-conduction mechanism. The behavior of *s* as a function of the temperature was used to interpret σ_{dc} versus temperature.

ACKNOWLEDGMENTS

The authors gratefully acknowledge the financial support of this research project by the University of Malaya in the form of a grant (contract grant number PS214/2009A). One of the authors (S.B.A.) thanks the Ministry of Higher Education and Scientific Research of the Kurdistan Regional Government for a scholarship.

REFERENCES

1. Itoh, T.; Mitsuda, Y.; Ebina, T.; Uno, T.; Kubo, M. *J. Power Sources* **2009**, *189*, 531.
2. Singh, T. H. J.; Bhat, S. V. *Bull. Mater. Sci.* **2003**, *26*, 707.
3. Zang, L.; Luo, J.; Guo, J.; Liu, H.; Ru, J. *Polym. Bull.* **2010**, *65*, 669.

4. Hema, M.; Selvasekarapandian, S.; Hirankumar, G.; Sakunthala, A.; Arunkumar, D.; Nithya, H. *J. Phys. Chem. Solids* **2009**, *70*, 1098.
5. Borgohain, M. M.; Joykumar, T.; Bhat, S. V. *Solid State Ionics* **2010**, *181*, 964.
6. Pradhan, D. K.; Choudhary, R. N. P.; Samantaray, B. K. *Mater. Chem. Phys.* **2009**, *115*, 557.
7. Deka, M.; Kumar, A. *J. Power Sources* **2011**, *196*, 1358.
8. Weston, J. E.; Steele, B. C. H. *Solid State Ionics* **1982**, *7*, 75.
9. Alloin, F.; D'Aprea, A.; El Kissi, N.; Dufresne, A.; Bossard, F. *Electrochim. Acta* **2010**, *55*, 5186.
10. Malathi, J.; Kumaravadivel, M.; Brahmanandhan, G. M.; Hema, M.; Baskaran, R.; Selvasekarapandian, S. *J. Non-Cryst. Solids* **2010**, *356*, 2277.
11. Prajapati, G. K.; Roshan, R.; Gupta, P. N. *J. Phys. Chem. Solids* **2010**, *71*, 1717.
12. Pradhan, D. K.; Choudhary, R. N. P.; Samantaray, B. K. *eXPRESS Polym. Lett.* **2008**, *2*, 630.
13. Sengwa, R. J.; Choudhary, S.; Sankhla, S. *Compos. Sci. Technol.* **2010**, *70*, 1621.
14. Singh, K. P.; Gupta, P. N. *Eur. Polym. J.* **1998**, *37*, 1023.
15. Shujahadeen, B. A.; Abidin, Z. H. Z.; Arof, A. K. *Phys. B: Condens. Matter* **2010**, *405*, 4429.
16. Shujahadeen, B. A.; Abidin, Z. H. Z. *Mater. Chem. Phys.* **2014**, *144*, 280.
17. Shujahadeen, B. A.; Abidin, Z. H.; Arof, A. K. *eXPRESS Polym. Lett.* **2010**, *4*, 300.
18. Ahmad, S.; Agnihotry, S. A. *Curr. Appl. Phys.* **2009**, *9*, 108.
19. Shujahahadeen, B. A.; Abidin, Z. H. Z. *J. Soft Matter* **2013**, *2013*, 8.
20. Raghavan, P.; Zhao, X.; Manuel, J.; Chauhan, G. S.; Ahn, J.-Y.; Ryu, H.-S.; Ahn, H.-J.; Kim, K.-W.; Nah, C. *Electrochim. Acta* **2010**, *55*, 1347.
21. Li, Z.; Su, G.; Wang, X.; Gao, D. *Solid State Ionics* **2005**, *176*, 1903.
22. Awadhia, A.; Agrawal, S. L. *Solid State Ionics* **2007**, *178*, 951.
23. Ramya, C. S.; Selvasekarapandian, S.; Hirankumar, G.; Savitha, T.; Angelo, P. C. *J. Non-Cryst. Solids* **2008**, *354*, 1494.
24. Shanmukaraj, D.; Wang, G. X.; Murugan, R.; Liu, H. K. *J. Phys. Chem. Solids* **2008**, *69*, 243.
25. Tan, C. G.; Siew, W. O.; Pang, W. L.; Osman, Z.; Chew, K. W. *Ionics* **2007**, *13*, 361.
26. Dissanayakea, M. A. K. L.; Jayathilakaa, P. A. R. D.; Bokalawalaa, R. S. P.; Albinssonb, I.; Mellander, B.-E. *J. Power Sources* **2003**, *119*, 409.
27. Karan, N. K.; Pradhan, D. K.; Thomas, R.; Natesan, B.; Katiyar, R. S. *Solid State Ionics* **2008**, *179*, 689.
28. Osińska, M.; Walkowiaka, M.; Zalewskab, A.; Jesionowski, T. *J. Membr. Sci.* **2009**, *326*, 582.
29. Patsidis, A.; Psarras, G. C. *eXPRESS Polym. Lett.* **2008**, *2*, 718.
30. Jiansirisomboon, S.; Watcharapasorn, A. *Curr. Appl. Phys.* **2008**, *8*, 48.
31. Shujahadeen, B. A.; Abidin, Z. H. Z. *J. Polymers* **2014**, *2014*, 9.
32. Petrowsky, M.; Frech, R. *J. Phys. Chem. B* **2009**, *13*, 5996.
33. Petrowsky, M.; Frech, R. *Electrochim. Acta* **2010**, *55*, 1285.
34. Dutta, A.; Sinha, T. P.; Jena, P.; Adak, S. *J. Non-Cryst. Solids* **2008**, *354*, 3952.
35. Hill, R. M.; Dissado, L. A. *J. Phys. C: Solid State Phys.* **1985**, *18*, 3829.
36. Sengwa, R. J.; Sankhla, S. *Polym. Bull.* **2008**, *60*, 689.
37. Bassiouni, M. E.; Al-Shamy, M. E. F.; Madi, N. K.; Kassem, M. E. *Mater. Lett.* **2003**, *57*, 1595.
38. Hema, M.; Selvasekarapandian, S.; Arunkuma, D.; Sakunthala, A.; Nithya, H. *J. Non-Cryst. Solids* **2009**, *355*, 84.
39. Potty, S. S. N.; Khadar, M. A. *Bull. Mater. Sci.* **2000**, *23*, 361.
40. Baskaran, R.; Selvasekarapandian, S.; Kuata, N.; Kawamura, J.; Hattori, T. *Solid State Ionics* **2006**, *177*, 2679.
41. Migahed, M. D.; Ishra, M.; Fahmy, T.; Barakat, A. *J. Phys. Chem. Solids* **2004**, *65*, 1121.
42. Yang, J.; Meng, J.; Shen, M. R.; Fang, L.; Wang, J. L.; Lin, T.; Sun, J. L.; Chu, H. J. *J. Appl. Phys.* **2008**, *104*, 104113.